Journal of Bioscience and Bioengineering
VOL. 128 No. 2, 226–233, 2019

ELSEVIER

www.elsevier.com/locate/jbiosc

Ultrasonically-guided flow focusing generates precise emulsion droplets for high-throughput single cell analyses

Colton E. Lagerman,[1] Sheila N. López Acevedo,[2] Ahmed S. Fahad,[2] Amen T. Hailemariam,[3] Bharat Madan,[2] and Brandon J. DeKosky[1,2,4,*]

Department of Chemical Engineering, The University of Kansas, Lawrence, KS 66044, USA,[1] Department of Pharmaceutical Chemistry, The University of Kansas, Lawrence, KS 66044, USA,[2] Department of Biochemistry, The University of Kansas, Lawrence, KS 66044, USA,[3] and Kansas Vaccine Institute, The University of Kansas, Lawrence, KS 66044, USA[4]

Received 7 December 2018; accepted 30 January 2019
Available online 20 March 2019

Emulsion-based techniques have dramatically advanced our understanding of single-cell biology and complex single-cell features over the past two decades. Most approaches for precise single cell isolation rely on microfluidics, which has proven highly effective but requires substantial investment in equipment and expertise that can be difficult to access for researchers that specialize in other areas of bioengineering and molecular biotechnology. Inspired by the robust droplet generation technologies in modern flow cytometry instrumentation, here we established a new platform for high-throughput isolation of single cells within droplets of tunable sizes by combining flow focusing with ultrasonic vibration for rapid and effective droplet formation. Application of ultrasonic pressure waves to the flowing jet provided enhanced control of emulsion droplet size, permitting capture of 25,000 to 50,000 single cells per minute. As an example application, we applied this new droplet generation platform to sequence the antibody variable region heavy and light chain pairings (VH:VL) from large repertoires of single B cells. We demonstrated the recovery of > 40,000 paired CDRH3:CDRL3 antibody clusters from a single individual, validating that these droplet systems can enable the genetic analysis of very large single-cell populations. These accessible new technologies will allow rapid, large-scale, and precise single-cell analyses for a broad range of bioengineering and molecular biotechnology applications.

[**Key words:** Single cell analysis; Emulsion; B cells; Microfluidics; Flow-focusing; Ultrasonic energy]

Single cell DNA and RNA sequencing technologies have had a major impact on diverse fields of biology in recent years, including microbiology, neurobiology, immunology and cancer research (1–3). As one example, single-cell sequencing provides a powerful approach to resolve microbial genomes and delineate cell-to-cell diversity with bacteria, yeasts, and algae as well as for detection and identification of pathogens (3–6). In neurobiology, single-cell gene expression patterns can determine the molecular profile of each individual cell that contributes to organ-level function and facilitate the quantification of the peripheral axonal growth state (7–11). Simultaneous profiling of the expression of many genes in a single cell is made possible by single cell isolation. Single cell sequencing methods have also been used for delineating clonal diversity as well as understanding the role of rare cells during cancer progression and have a major impact on improving our fundamental understanding of intratumor heterogeneity, drug screening, clonal evolution and metastatic dissemination in human cancers (12–17).

Our work has focused on understanding the complexity of immune responses, and single-cell approaches are critical for improved insights in adaptive and innate immunity (18–22). Single-cell technology enables the analysis of immune signaling and cell migration, facilitates antibody screening, and allows massively parallel analysis of B- and T-cell repertoires (21). Microfluidics has proven to be effective for dynamic monitoring of immune cells with a high degree of control over the cellular microenvironment, allowing scientists to account for the diverse behavior of immune cells that cannot be resolved using bulk study methods (18,21–25).

The earliest emulsion-based, single-cell systems applied shear stress generated by conventional mixing or vortexing to isolate single genes or single cells into emulsion droplets for high-throughput screening purposes (26–30). These platforms provided a major boost to single-cell technologies and continue to have significant research and industrial applications, particularly in the analysis of DNA, enzymes, and single bacterial cells. However, the wide range of droplet sizes generated by mixing-based droplet isolation limits the consistency of reactions between droplets. Shear stress can also damage fragile mammalian cell walls (31). Other technologies capture single cells into 2-dimensional printed microwells using a variety of formats (32–36). These 2D capture technologies provide highly effective single cell interrogation platforms with advantages in reagent exchange and analysis but remain limited in cell throughput because the 2D nature of printed microwell platforms restricts the number of cells that can be analyzed (generally $<10^5$ single cells per experiment).

* Corresponding author at: Department of Chemical, Engineering Department of Pharmaceutical Chemistry, The University of Kansas, 2095 Simons Biosciences Research Labs, Room 158, Lawrence, KS 66044, USA. Tel.: +1 785 864 2468.
E-mail address: dekosky@ku.edu (B.J. DeKosky).

1389-1723/$ – see front matter
https://doi.org/10.1016/j.jbiosc.2019.01.020

In recent years, microfluidic-based platforms have become a predominant method for single-cell capture and isolation. A variety of microfluidic platforms have been developed and applied for single-cell analyses, including continuous flow systems, which are commonly used for studying and analyzing the behavior of migrating cells (37–40). Nanowells and droplet-based methods are commonly used for measuring the amount of antibody produced by individual B cells and characterizing surface marker expression in rare populations of cells (35,41,42). Valve-based microfluidics can process and profile single-cell transcriptional information, for example, uncover rare immune cell states (43), survey neuronal diversity (44), and assess cellular hierarchy within lung epithelia (45). Thus, while the field has been dominated by protocols involving the sorting of tens to hundreds of single cells into multiwell plates using fluorescence activated cell sorting (FACS) (46–48), many scientists and bioengineers have recently embraced droplet- and nanowell-based approaches for studying and profiling thousands of cells in parallel. However, the fabrication and experimental implementation of these chip-based devices can be complex and time-consuming and requires specialized expertise that is not commonly available in laboratories without a dedicated focus in microengraving and microfluidic technologies. The throughput of these systems can be a limiting factor for analyzing human samples, as processing millions of cells can take many hours to complete and may be impractical for fresh cells from clinical samples (21,41,49). New technologies for rapid, precise, and accessible single-cell isolation could provide new ways for researchers in molecular biology to quickly perform single-cell assays on large biological samples.

In addition to shear forces generated by mixing or microfluidic flow, mechanical (often ultrasonic) waves can be applied to a liquid stream as another means of controlling droplet breaking points and minimizing variability in emulsion size. Mechanical forces for droplet isolation have been utilized in fluorescence-activated cell sorting (FACS) for many years (50,51). In these systems, low-power mechanical waves are applied to vibrate a nozzle assembly that cells, along with a sheath fluid, pass through to generate uniformly sized droplets. These controlled forces allow stabilized droplets to form at a precise point before droplet separation using an electrostatic field (51,52). While mechanical vibration has been applied extensively in commercial flow cytometry equipment, such mechanical forces have not yet been broadly applied for single-cell isolation inside emulsion droplets.

To address limitations posed by available technologies, previously we outlined a new emulsion-based workflow for the rapid and effective analysis of paired heavy:light antibody sequencing from >5 million single human B cells per experiment (53,54). This system isolated single cells along with lysis buffer and magnetic beads for mRNA capture into droplets of a predictable size distribution. The systems were shown to be highly effective and accurate, with some acceptable variation in droplet sizes (53,54). For broader single-cell applications, we sought to achieve enhanced control of droplet sizes and thus control various critical features of single-cell reactions including the concentration of cells per droplet and the availability of reactants (e.g., magnetic beads, total reaction volume, enzyme quantities). An instrument rapidly producing tunable droplet sizes would permit enhanced optimization of single-cell reactions. Inspired by the mechanical droplet isolation technologies of modern flow cytometry, we hypothesized that the incorporation of ultrasonic energy as used in FACS could combine with our flow focusing droplet generation systems to further enhance control of single-cell isolation. We combined ultrasonic pressure with a flow-focusing jet to control emulsion droplet breakoff points, resulting in tunable droplet sizes for single-cell studies. As an example analysis, we then applied these new droplet generation technologies for single-cell genetic characterization of large B cell repertoires, demonstrating utility in a relevant system for molecular biotechnology. The simplicity of device assembly and operation, the comparatively large volumetric flow rates, and our ability to carry out high-throughput analysis of millions of individual mammalian cells in a massively parallel manner makes our emulsion microfluidics platform an effective new single-cell analysis tool to accelerate the study of single cell behavior in modern biotechnology.

MATERIALS AND METHODS

Ultrasonically-guided flow focusing device construction A flow focusing nozzle was built as described previously (54). Briefly, two concentric needles, one 19-gauge and one 26-gauge needle were housed within a melted and sanded borosilicate glass nozzle with an orifice of ~150 μm. To control droplet breakoff points, we incorporated ultrasonic vibrations using a piezoelectric transducer (Sonics & Materials, Newtown, CT, USA) driven by an amplifier (Trek, Lockport, NY, USA); a schematic is shown in Fig. 1. The output wave frequency and amplitude were controlled by a digital function generator (Keysight, Santa Rosa, CA, USA) (Fig. 1). The transducer tip was clamped directly to the nozzle metal reaction tee housing to propagate waves through the liquid jet. A dual syringe pump (KD Scientific Legato 200, KD Scientific, Holliston, MA, USA) was used to drive aqueous solutions while an M50 gear pump (Valco Instruments, Houston, TX, USA) was used to pump the carrier oil stream into the glass nozzle surrounding the needles, focusing aqueous streams into a high velocity jet through the nozzle orifice. A camera system consisting of a Basler acA1300-200uc camera (Basler, Exton, PA, USA), VZM 1000I zoom imaging lens (cat. No. NT55-834, Edmund Optics, Barrington, NJ, USA), and rack and pinion coarse movement (cat. No. NT03-609, Edmund Optics) was mounted on a ring stand and used to observe fluid flow within the glass nozzle, as previously reported (54). We applied this camera system to visualize emulsion formation at the droplet breakoff point, which was found to be 3–5 cm below the nozzle under conditions reported here.

Emulsion preparation and analysis PBS and lysis buffer (100 mM Tris pH 7.5, 500 mM LiCl, 10 mM EDTA, 1% lithium dodecyl sulfate, 5 mM DTT) were prepared as the two aqueous streams, placed into separate 5–20 mL syringes, and pumped through the emulsification system described above. A carrier oil stream (4.5% (v/v) Span 80, 0.4% (v/v) Tween 80, and 0.05% (v/v) Triton X-100 in mineral oil) was flowed around the aqueous streams. Emulsions were collected using a 2 mL Eppendorf tube or a 50 mL centrifuge tube approximately 5 inches below the nozzle exit. Collected emulsions were examined on a hemocytometer (Neubauer) using an Olympus IX70 microscope attached to a Nikon D5300 camera controlled using

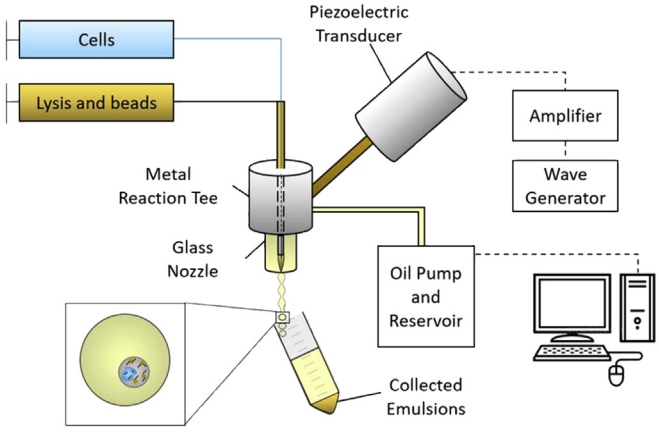

FIG. 1. A schematic of the single-cell emulsion generation device that incorporates both flow focusing and mechanical wave generation. For performing single-cell mRNA capture, cells suspended in PBS and lysis buffer with magnetic beads to capture mRNA are fed by a syringe pump into two concentric needles. An oil phase is fed by a gear pump into a glass nozzle that focuses the flow of the two aqueous streams into a nozzle orifice. The dual needle and glass nozzle assembly is housed inside a metal reaction tee, and a piezoelectric transducer applies mechanical waves to control droplet breakoff points. The transducer is driven by a wave generator and amplifier system. Falling single-cell emulsion droplets are collected in 50 mL tubes; cell lysis and mRNA capture takes place inside the emulsion droplets for downstream purification and analysis.

Control My Nikon v.5.3 software (Tetherscript Technology Corporation, Vancouver, Canada). Emulsion droplet diameters were assessed using ImageJ (NIH) by measuring at least 200 emulsion droplets.

As a comparison, we also generated emulsions using conventional mixing. A solution of 0.25 mL 0.4% Trypan Blue in PBS (Sigma–Aldrich, St. Louis, MO, USA), 0.25 mL PBS, 0.5 mL lysis buffer (100 mM Tris pH 7.5, 500 mM LiCl, 10 mM EDTA, 1% lithium dodecyl sulfate, 5 mM DTT) and 3 mL of oil phase solution (molecular biology grade mineral oil with 4.5% Span-80, 0.4% Tween 80, 0.05% Triton X-100, v/v %, Sigma Aldrich Corp.) was prepared and mixed gently by inverting the solution in a 5 mL Falcon tube three times. The resulting emulsion mixture was placed on a hemocytometer and analyzed via light microscopy with an Olympus IX70 attached to a Nikon D5300 camera using Control My Nikon v.5.3 software (Tetherscript Technology Corporation, Fig. S1). ImageJ post-processing was used to measure droplet diameters.

Cell preparation We used Jurkat cells as a model cell line to test cell viability and determine optimal cell concentrations. Jurkat cells (kind gift of Daniel C. Douek, Vaccine Research Center, NIAID/NIH) were maintained in complete RPMI (Thermo Fisher Scientific, NY, USA) at 37°C in 5% CO_2. Cells were centrifuged at 300 $\times g$ for 10 min and the supernatant was removed from the pellet before resuspension in 1 mL of PBS. Cells were counted using a hemocytometer and diluted as necessary to study the effects of cell concentration on emulsification. Cell viability was determined to be > 98% for all samples. The resuspended cells were pumped through the inner stream of the device, and cell viability was measured after applying wave generation by observing the fraction of cells stained by 0.4% Trypan Blue (Life Technologies, Carlsbad, CA, USA). In some experiments, live Jurkat cells were divided into two equal groups, with one group consisting of killed cells as a nonviable cell control. In these experiments, the killed cell group was subjected to 60°C for 30 min in a heat block to induce cell death, while the other group was treated normally.

mRNA quantification To first visualize mRNA capture beads, poly(dT) magnetic beads (1.0 μm diameter, New England Biosciences, Ipswich, MA, USA) were tagged with poly(A)-fluorescein (5' 6-FAM, IDT, Skokie, IL, USA). Poly(dT) beads were then encapsulated in droplets using the flow focusing device and the droplets were viewed on a hemocytometer using a Nikon Diaphot microscope attached to a Nikon D5300 camera controlled by Control My Nikon v.5.3 software (Tetherscript Technology Corporation).

Next, Jurkat cells were used to compare mRNA capture efficiency with and without wave-assisted droplet formation. Poly(dT) magnetic beads were pelleted and resuspended in cell lysis/binding buffer, and the cell solution and lysis/beads mixture were passed at 0.5 mL/min while oil phase (4.5% v/v Span 80, 0.4% v/v Tween 80, and 0.05% v/v Triton X-100 in mineral oil) was pumped through the outermost glass tubing at 3 mL/min in the absence of mechanical waves. When wave generation was used, solutions were run at 0.04 mL/min aqueous phase and 4.5 mL/min oil phase with wave frequency of 6.5 kHz and amplitude of 2.5 V peak to peak (V_{PP}). In both cases, the emulsified stream was collected into 50-mL Falcon tubes, which were placed on ice for a maximum of forty-five minutes. Tubes were centrifuged at 4000 rpm for 5 min at 4°C, and the upper mineral oil layer was discarded. An equal volume of cold hydrated diethyl ether was added to break the emulsions, and tubes were centrifuged again at 4000 rpm for 5 min at 4°C to pellet the magnetic beads. The supernatant was removed, and pelleted beads were washed with 1 mL of cold wash buffer (100 mM Tris pH 7.5, 500 mM LiCl, 1 mM EDTA). They were then pelleted using a magnet and resuspended in 2 mL cold lysis/binding buffer (100 mM Tris pH 7.5, 500 mM LiCl, 10 mM EDTA, 1% LiDS, 5 mM DTT). Beads were washed again with 1 mL of cold wash buffer before being placed into molecular biology grade water. mRNA was eluted from the beads using a heat block at 90°C for 2 min, and magnetic beads were discarded. A Thermo Scientific NanoDrop One Microvolume UV–Vis Spectrophotometer (Thermo Fisher Scientific) was used to determine the mRNA concentration and evaluate mRNA recovery.

Antibody analysis of memory B cell populations PBMCs were isolated from donated human whole blood after informed consent was obtained (Gulf Coast Regional Blood Center, Houston, TX, USA). Non-B cells were depleted by magnetic bead separation, and $CD27^+$ antigen-experienced B cells were isolated by positive magnetic bead separation (EasySep Human B cell enrichment kit w/o CD43 Depletion, STEMCELL Technologies, Vancouver, Canada, and CD27 Human Microbeads, Miltenyi Biotec, Auburn, CA, USA). Antigen-experienced B cells (hereafter referred to as memory B cells) were stimulated *in vitro* for 5 days to enhance antibody gene transcription. Cells were incubated 5 days in the presence of Iscove's Modified Dulbecco's Medium (IMDM) (Thermo Fisher Scientific) supplemented with 10% FBS, 1 × GlutaMAX, 1 × non-essential amino acids, 1 × sodium pyruvate and 1 × penicillin/streptomycin (Life Technologies) along with 100 units/mL IL-2 and 50 ng/mL IL-21 (PeproTech, Rocky Hill, NJ, USA). B cells were co-cultured with irradiated 3T3-CD40L fibroblast cells that secrete CD40L (kind gift of John Mascola, Vaccine Research Center, NIAID) to aid B cell expansion. Images were taken of the cultures during the 5 days of B cell expansion via light microscopy using the Olympus IX70 microscope (Fig. S2, Table S1). Memory B cells were emulsified as previously described (53), either with or without the application of mechanical waves. Briefly, for emulsions generated in the absence of mechanical waves the memory B cells were resuspended in PBS at a concentration of 100 k/mL and passed through the innermost, 19-gauge needle of the flow focusing device at 500 μL/min poly(dT) magnetic beads (1.0 μm diameter, New England Biosciences, Ipswich, MA, USA) were pelleted and resuspended in cell lysis/binding buffer (100 mM Tris pH 7.5, 500 mM LiCl, 10 mM EDTA, 1% lithium dodecyl sulfate, 5 mM DTT) at a concentration of 45 μL magnetic bead stock/mL lysis/binding buffer. The cell lysis/beads mixture was passed at 500 μL/min while oil phase (molecular biology grade mineral oil with 4.5% Span-80, 0.4% Tween 80, 0.05% Triton X-100, v/v%, Sigma Aldrich Corp.) was passed through the outermost glass tubing at 3 mL/min. In the presence of mechanical waves, the same conditions were applied with the addition of a wave frequency of 4 KHz and amplitude of 2.5 Vpp. The emulsified stream was collected into a series of 50-mL Falcon tubes, and each tube was placed on ice for a maximum of forty-five minutes. Magnetic beads were recovered as described previously and resuspended in an overlap-extension RT-PCR emulsion (53–55), using the RTX enzyme (kind gift of Andrew Ellington, UT–Austin) (56). Thermal cycling was performed under the following conditions: 30 min at 68°C followed by 2 min at 94°C; 40 cycles of 94°C for 30 s, 60°C for 30 s, 68°C for 2 min; 68°C for 7 min; held at 4°C. cDNA was extracted and a nested PCR was performed under the following conditions: 2 min at 94°C; 23 cycles of 94°C for 30 s, 64°C for 30 s, 72°C for 20s; 72°C for 7 min; held at 4°C (Kapa HiFi HotStart PCR Kit, Kapa Biosystems, Wilmington, MA, USA). Nested PCR product was electrophoresed to purify ~850 bp-linked transcripts and sequenced via Illumina 2 × 300 bp sequencing (33,53,54).

Bioinformatic analysis Illumina Miseq 2 x 300 sequence data was analyzed to identify the VH:VL gene repertoires as previously described (53). Briefly, Illumina sequences were quality-filtered, followed by V-(D)-J gene identification and CDR3 annotation using IgBLAST (57). Sequences with out-of-frame V(D)J recombination were excluded and productive sequences were paired by Illumina ID and compiled by exact CDR3 nucleotide match. Clustering of CDRH3 nt sequences were performed using vsearch v2.4.3 (58) to 96% nt identity with terminal gaps ignored; VH:VL nucleotide sequence pairs with less than 2 reads were excluded. VH:VL pairing precision, *P*, was calculated by computing the number of VH that paired with same VL in both replicates (true positives, *TP*), and VH that paired with a different VL across replicates (false positive, *FP*, in at least one replicate). *P* for a single analysis was calculated as previously described (53). Spearman rank correlation analysis of paired VH:VL gene usage was performed for the top 500 heavy and light variable gene pairs using Microsoft Excel. The raw sequence read data are available from the NCBI SRA with accession number PRJNA523171.

RESULTS

Generation of emulsions with precise control of droplet size We determined the impact of flow rates and wave frequency on droplet sizes by analyzing aqueous stream flow rate conditions between 0.04 and 0.5 mL/min, oil flow rates between 3.0 and 4.5 mL/min, and wave frequencies between 4 and 6.5 kHz (Table 1). We observed that aqueous streams within the nozzle narrowed at lower aqueous:oil flow rate ratios, indicating that varying flow rate was one parameter that we could use to adjust the aqueous stream thickness and control droplet size (Fig. 2). However, we were unable to obtain a substantial degree of control of droplet sizes by adjusting flow rates alone, and thus another means of control was necessary for generating high-precision droplets. With flow focusing alone in the absence of mechanical waves, emulsions showed droplet sizes of 75 ± 29 μm (average ± s.d., Table 1, Fig. 3).

We found that ultrasonic waves generated consistent droplets for wave frequencies between 4 and 7 kHz (Table 1). We identified several conditions that generated stable, uniform jet stream breaking points (Fig. 2C). Images of our system were strikingly similar to those captured by a Becton–Dickinson FacsAria III

TABLE 1. Emulsification settings for generation of a range of tunable droplet sizes.

Emulsification condition	1	2	3	4	5
Diameter (μm)	75 ± 29	101 ± 9	72 ± 9	51 ± 4	33 ± 4
Avg. droplet volume (nL)	0.22	0.54	0.2	0.07	0.02
Droplets/min	2.28E6	1.00E6	2.04E6	2.16E6	2.10E6
Aqueous flow rate (mL/min)	0.5	0.5	0.4	0.15	0.04
Oil flow rate (mL/min)	3.0	3.0	3.5	4.0	4.5
Wave frequency (kHz)	None	4.0	6.0	6.5	6.3

Droplet diameters are reported as average ± standard deviation.

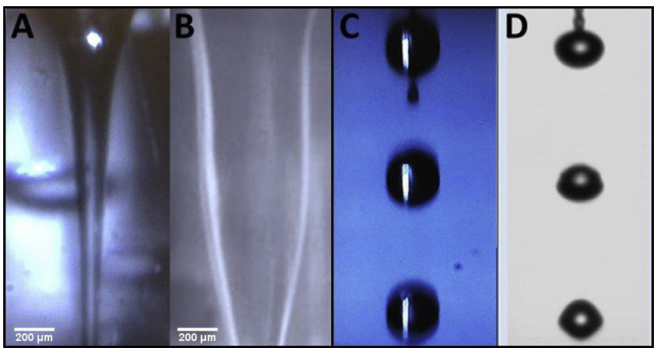

FIG. 2. Visual impact of system parameters on the flowing streams produced via droplet generation. Images of aqueous streams inside the glass nozzle were captured at (A) 0.04 mL/min compared to (B) 0.5 mL/min. The scale bar is 200 μm. (C) A micrograph of the droplet stream approximately 10 mm below the nozzle exit. (D) As a comparison, aqueous droplets formed just below the nozzle exit in a BD FACS-AriaII instrument.

fluorescence-activated cell sorting (FACS) instrument (Fig. 2D), suggesting that we had replicated similar droplet generation mechanisms from flow cytometry in our flow focusing device. Standard deviation in droplet sizes reduced from 29 μm in the absence of mechanical vibration to 9 μm when mechanical vibration was applied (Table 1, condition 2 and Fig. 3). The flow rates and mechanical waves investigated here led to the generation of uniform emulsion droplets with tunable diameters ranging from 33 ± 4 μm to 101 ± 9 μm (Table 1, Fig. 3). Thus, mechanical vibration enabled precise control of droplet breaking points to generate highly uniform emulsion droplets.

In general, emulsion volume increased at higher aqueous flow rates and decreased at higher oil flow rates, consistent with our observations of aqueous stream thickness (Fig. 2). Emulsion volume was tunable over an order of magnitude, with emulsion volumes ranging from 0.02 nL at an aqueous flow rate of 0.04 mL/min to 0.54 nL at an aqueous flow rate of 0.5 mL/min (Table 1). Emulsion diameter standard deviation was less than 12% of the mean emulsion diameter at each setting that incorporated mechanical waves. A correlation was developed relating droplet diameter to the aqueous flow rate and wave frequency, which are related by the Rayleigh instability equations (Fig. S3) (59,60).

To compare with our microfluidic technologies, we also generated emulsions of a similar average diameter using conventional mixing. We prepared a solution composed of trypan blue, PBS, lysis buffer and oil phase followed by inverting the tubes three times to the point of emulsion formation. The resulting emulsion was placed on a hemocytometer and analyzed via light microscopy. As expected, conventional mixing generated emulsions with a broad droplet dispersity and sizes that were difficult to control. We found that conventional mixing techniques would have limited utility for single-cell applications requiring droplets of approximately 100 μm diameter (Fig. S1).

Single cell encapsulation Next, we evaluated the capacity of our new droplet generation system to encapsulate viable cells for single-cell analysis. Mechanical vibration does not have a detrimental effect on cell viability in modern FACS instruments; however, we still wanted to verify that our system incorporating mechanical vibrations could encapsulate viable single cells. Jurkat cells were suspended at 1 million cells/mL in an aqueous solution consisting of a 50:50 mixture of PBS and 0.4% Trypan blue. Both live Jurkat cells and a dead cell control were emulsified using the ultrasonically guided flow-focusing device and viewed on a hemocytometer. We observed that cells emulsified by our device remained fully viable without altering the size distribution of the emulsions or the distribution of cells within emulsions (Fig. 4A), whereas dead cells that were killed by heating prior to emulsification stained blue as expected (Fig. 4B). At optimized cell distributions, approximately 1 in 50 emulsions contained single cells, which provided approximately 99% of cells as single cells in droplets by Poisson statistics.

Quantification of poly(dT) beads and mRNA recovery We next optimized the concentration of poly(dT) beads inside emulsion droplets using low flow conditions (0.04 mL/min aqueous). Magnetic poly(dT) beads were tagged with poly(A)-fluorescein to visualize the distribution of beads in emulsions. Each emulsion should contain at least 5–8 beads to ensure that all encapsulated

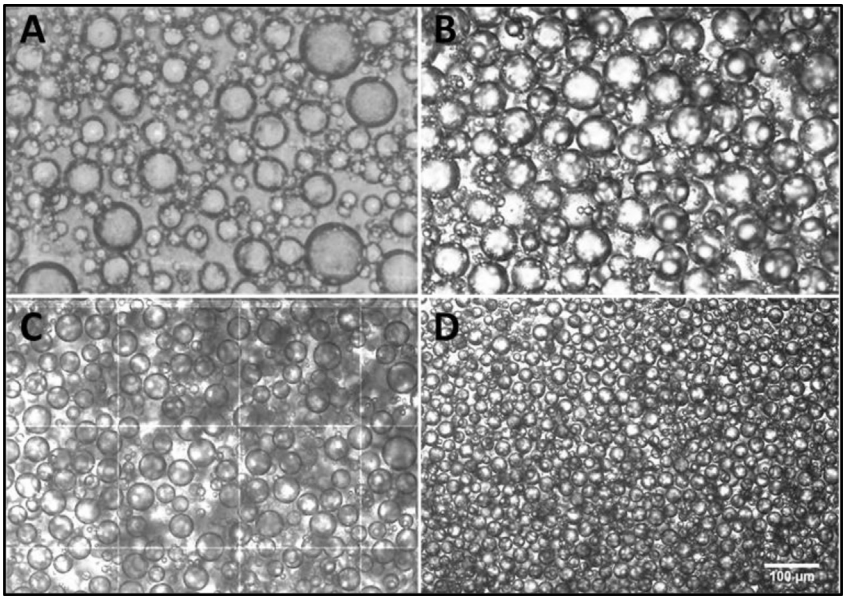

FIG. 3. Micrographs of emulsions generated using the flow-focusing device. (A) Emulsion droplets generated without wave generation. Droplet diameter was 75 ± 29 μm (average ± standard deviation) (condition 1, Table 1). (B) With wave generation at 6.0 Hz (condition 3). Emulsion diameter was 72 ± 9 μm. (C) With wave generation at 6.5 Hz (condition 4). Emulsion diameter was 51 ± 4 μm. (D) With wave generation at 6.3 Hz (condition 5). Emulsion diameter was 33 ± 4 μm. The scale bar is 100 μm for all panels.

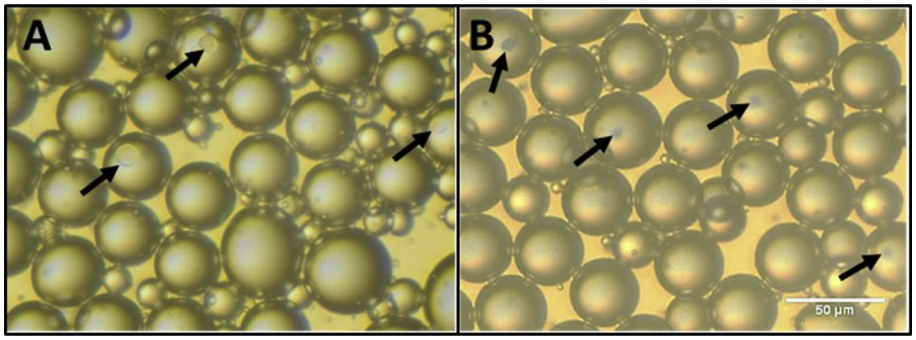

FIG. 4. Jurkat cells were encapsulated in emulsions formed using wave generation to evaluate effects of wave generation on cell viability. A solution of 0.4% trypan blue was utilized in place of lysis buffer to determine cell viability after droplet generation. (A) Jurkat cells after the single-cell emulsification process. (B) Pre-killed Jurkat cells after emulsification. The scale bar is 50 μm for both panels.

cells are subjected to similar mRNA capture conditions; however, too many beads in solution could lead to bead clumping and decreased emulsion performance. We found an optimal bead concentration to be 1 mg beads/mL lysis buffer; the bead distribution is shown in Fig. S4. At this concentration, almost all emulsions contained beads and the emulsion size distribution was negligibly affected.

To quantify the amount of captured mRNA with mechanical vibrations applied, the flow focusing device was used in the absence of any mechanical vibration as a control (Table 1, condition 1), and with wave generation applied (Table 1, condition 5). In condition 1, 1 million Jurkat cells in 10 mL PBS were lysed with 450 μg poly(dT) beads in 10 mL lysis buffer without wave generation. At an emulsification rate of 50,000 cells/min, this process required 20 min. Emulsions were collected in 50 mL tubes and stored on ice for 45 min as mRNA from lysed single cells annealed to magnetic beads. While the emulsions from condition 1 were maintained on ice, the flow focusing device was ran again using condition 5 with 1 million Jurkat cells isolated from the same culture. Poly(dT) beads in lysis buffer (1 mg/mL) were flowed in parallel for emulsification with the cells; emulsification for condition 5 required approximately 25 min. Magnetic beads with annealed mRNA were washed and mRNA was eluted from the beads and quantified by spectrophotometry. Table 2 shows a comparison of mRNA captured at each condition. In all trials, the difference in mRNA captured with and without wave generation was a maximum of 11%, indicating that the inclusion of mechanical vibrations did not have a substantial negative impact on mRNA recovery. Initial trials that utilized a non-optimized concentration of mRNA capture beads (450 μg/mL lysis buffer) in both conditions led to mRNA capture decreases of up to 27%, demonstrating the importance of higher concentrations of mRNA beads at smaller droplet sizes (Table S2).

Single B cell paired VH:VL gene analysis We tested the ability of our droplet generation system to perform a single-cell analysis on human cell samples. In this experiment, we analyzed the paired heavy and light chain sequences from repertoires of human B cells, which each contain a distinct heavy and light chain antibody gene (61,62). We isolated human memory B cells from PBMCs from a healthy human donor and expanded the cells for 5 days *in vitro* by stimulation with IL-2, IL-21, and co-cultured with 3T3-CD40L fibroblasts. Memory B cells were observed throughout stimulation via light microscopy (Fig. S2), demonstrating that B cells were expanding in culture. *In vitro* cell expansion enhanced antibody transcription and generated a population of expanded B cells to assess the accuracy of our technique (Table S1). We analyzed 2 million total *in vitro* stimulated B cells and ran them through the flow-focusing device at a rate of 50,000 cells per minute. These cells were divided in two: 1 million cells were emulsified without mechanical vibration as in condition 1, whereas the other 1 million cells were emulsified in the presence of mechanical vibration as shown in condition 5 (Table 1). After collecting the resulting emulsions and performing overlap extension RT-PCR as described (33,54,63), we amplified the resulting cDNAs by nested PCR to generate a ~850-bp VH:VL product for high-throughput sequencing. We sequenced FRH4-(CDR-H3)-FRH3:FRL3-(CDR-L3)-FRL4 antibody regions to reveal the single-cell pairings between the VH and VL hypervariable loops. We recovered more than 40 k heavy:light clusters per 1 million cell sample. Antibody variable gene (V-gene) usage was highly diverse in our recovered single-cell sequence libraries and included several rarely expressed antibody V-genes, demonstrating that the large number of single cells were analyzed (Fig. 5). V-gene usage in these samples was consistent with prior reports (33,53,55) and showed a VH:VL pairing precision of 92.0%, validating that this technology allows with high precision the natively paired antibody sequences from millions of single B cells. The paired VH:VL gene usage of the sample treated with conditions 1 and 5 were highly correlated (Spearman $\rho = 0.906$, p-value: 1.91×10^{-187}). These data show that the use of mechanical waves for precise single-cell droplet generation can be applied for effective single-cell genetic analysis.

TABLE 2. Quantification of mRNA from single Jurkat cells encapsulated by our single-cell isolation platform.

	mRNA captured (ng)		Difference (%)
	Flow focusing device	Ultrasonically-guided flow focusing	
Trial 1	471 ± 8.0	435 ± 7.0	7.6
Trial 2	470 ± 15	460 ± 11	2.1
Trial 3	425 ± 9.0	380 ± 8.0	11

Two million Jurkat cells were analyzed for each trial (1 million for flow focusing alone and 1 million for flow focusing with ultrasonic guidance). Values are reported as average ± standard deviation; three mRNA concentration measurements were performed for each trial.

DISCUSSION

Inspired by the robust droplets generation technologies of modern flow cytometry platforms, we established a flexible new system to generate precise water-in-oil emulsion droplets of tunable sizes for single-cell analyses in bioengineering and biotechnology. By combining mechanical vibration with flow-focusing droplet generation technologies, this new system easily can obtain precise droplets of varying sizes and constitutes a flexible tool for single cell studies. The emulsions generated here spanned over an order of magnitude in droplet volumes

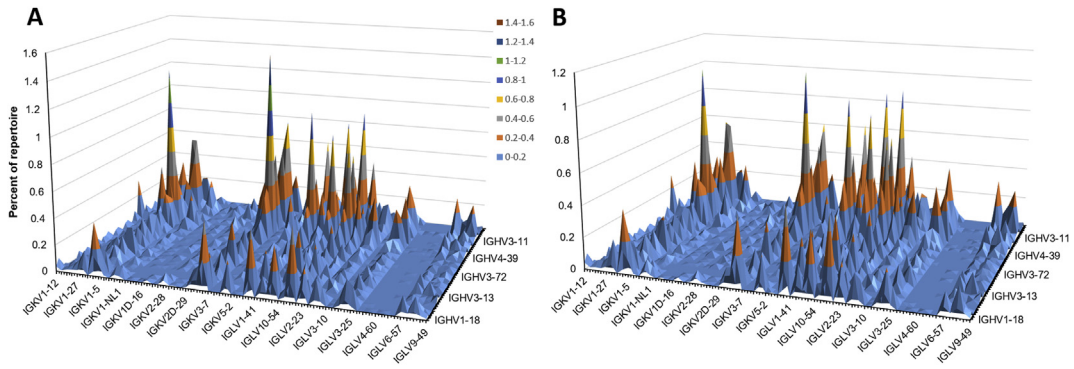

FIG. 5. Paired heavy and light variable gene usage. Surface plots for the paired heavy and light V-gene usage of the sample treated with (A) condition 1 and (B) condition 5 (Table 1). Height of the peak represents the percentage of a VH:VL gene pair among the sequenced repertoire.

(0.02–0.54 nL), which is in the appropriate range for most prokaryotic and eukaryotic single-cell applications. Our additional ability to mix two concurrent aqueous streams at the point of droplet formation allows for a broad range of applications, for example to mix a cell stream with PCR reagents, protein detection reagents, or lysis buffer for gene capture as we have shown here. These systems can be built and operated by most researchers in bioengineering or molecular biotechnology, as our platform allows very high cell throughput and effective emulsion generation without requiring sophisticated microfabrication and microengraving equipment or expertise. We reported emulsification of up to 30 mL aqueous phase per hour, generating up to 140 million droplets per hour, which is substantially higher than most comparable microfluidic platforms. As with other microfluidic devices, these systems could be operated in parallel for further increases in single cell throughput if desired (64,65).

We observed that emulsion droplet sizes were highly predictable but had a comparatively broader size distribution when we used flow focusing alone without mechanical vibration to control droplet formation. In contrast, we found that mechanical waves greatly reduced droplet size variance and allowed for precise control of droplet sizes. Such fine control of droplet size is important for several reasons. First, emulsion stability is highly dependent on droplet size: smaller droplets are kinetically stable whereas larger emulsion droplets can cause droplet coalescence; thus, emulsions with controlled droplet size behave more predictably and permit more robust experiments in lab settings. Reduced emulsion size variability also enhances uniformity for increased control of emulsion contents. This higher degree of control can reduce inherent bias in systems such as bias that results from PCR amplification in polydisperse droplets (66,67). Precise control of droplet size as we have shown here can also enhance reagent efficiency by minimizing droplet size and reagent volumes as needed, and cell and reagent concentrations can be optimized to achieve desired concentrations. We showed that these modifications can be made without sacrificing cell viability or the total amount of mRNA isolated from cells, and with minimal impact to cell throughput (Tables 1 and 2). The addition of wave generation also enhances the control of rare features such as multiple cells per droplet. The high degree of droplet size control and the tunable range of droplet volumes should enable our platform to be utilized in a broad range of applications requiring monodisperse emulsions.

Nozzle geometry can also have a strong influence on droplet sizes. As the orifice diameter changes, the stream velocity (and therefore thickness) changes accordingly. Adjusting the nozzle orifice diameter could increase the range of emulsion sizes that are achievable and may be the focus of future studies. These and other tunable features of our platform allow for enhanced flexibility along with high throughput compared to alternative single-cell emulsification methods, and we demonstrated its application for performing high-precision analysis of large repertoires of paired B cell receptors. The flexible droplet generation systems that we describe here offer an accessible and versatile platform to enable large-scale single cell isolation in a broad range of precision single-cell studies in biotechnology and bioengineering.

Supplementary data to this article can be found online at https://doi.org/10.1016/j.jbiosc.2019.01.020.

ACKNOWLEDGMENTS

We thank Joe Taft for assistance with BD FacsAria III operation. We also thank John R. Mascola, Vaccine Research Center, NIAID/NIH for 3T3-msCD40L cells and Daniel C. Douek, Vaccine Research Center, NIAID/NIH for Jurkat cells. This work was supported by the University of Kansas Departments of Pharmaceutical Chemistry and Chemical Engineering and by NIH grants 1DP5OD023118, P20GM113117, and P20GM103638.

References

1. **Armbrecht, L. and Dittrich, P. S.:** Recent advances in the analysis of single cells, Anal. Chem., **89**, 2–21 (2017).
2. **Gao, D., Jin, F., Zhou, M., and Jiang, Y.:** Recent advances in single cell manipulation and biochemical analysis on microfluidics, Analyst, **144**, 766–781 (2019).
3. **Hu, P., Zhang, W., Xin, H., and Deng, G.:** Single cell isolation and analysis, Front. Cell Dev. Biol., **4**, 116 (2016).
4. **Cottinet, D., Condamine, F., Bremond, N., Griffiths, A. D., Rainey, P. B., de Visser, J. A., Baudry, J., and Bibette, J.:** Lineage tracking for probing heritable phenotypes at single-cell resolution, PLoS One, **11**, e0152395 (2016).
5. **Kaminski, T. S., Scheler, O., and Garstecki, P.:** Droplet microfluidics for microbiology: techniques, applications and challenges, Lab Chip, **16**, 2168–2187 (2016).
6. **Potvin-Trottier, L., Luro, S., and Paulsson, J.:** Microfluidics and single-cell microscopy to study stochastic processes in bacteria, Curr. Opin. Microbiol., **43**, 186–192 (2018).
7. **Bota, M. and Swanson, L. W.:** The neuron classification problem, Brain Res. Rev., **56**, 79–88 (2007).
8. **Fishell, G. and Heintz, N.:** The neuron identity problem: form meets function, Neuron, **80**, 602–612 (2013).
9. **Jocher, G., Mannschatz, S. H., Offterdinger, M., and Schweigreiter, R.:** Microfluidics of small-population neurons allows for a precise quantification of the peripheral axonal growth state, Front. Cell. Neurosci., **12**, 166 (2018).
10. **Poulin, J.-F., Tasic, B., Hjerling-Leffler, J., Trimarchi, J. M., and Awatramani, R.:** Disentangling neural cell diversity using single-cell transcriptomics, Nat. Neurosci., **19**, 1131–1141 (2016).

11. **Trapnell, C.:** Defining cell types and states with single-cell genomics, Genome Res., **25**, 1491–1498 (2015).
12. **Anguiano, M., Castilla, C., Maska, M., Ederra, C., Pelaez, R., Morales, X., Munoz-Arrieta, G., Mujika, M., Kozubek, M., Munoz-Barrutia, A., and other 4 authors:** Characterization of three-dimensional cancer cell migration in mixed collagen-Matrigel scaffolds using microfluidics and image analysis, PLoS One, **12**, e0171417 (2017).
13. **Eduati, F., Utharala, R., Madhavan, D., Neumann, U. P., Longerich, T., Cramer, T., Saez-Rodriguez, J., and Merten, C. A.:** A microfluidics platform for combinatorial drug screening on cancer biopsies, Nat. Commun., **9**, 2434 (2018).
14. **Francis, J. M., Zhang, C. Z., Maire, C. L., Jung, J., Manzo, V. E., Adalsteinsson, V. A., Homer, H., Haidar, S., Blumenstiel, B., Pedamallu, C. S., and other 4 authors:** EGFR variant heterogeneity in glioblastoma resolved through single-nucleus sequencing, Cancer Discov., **4**, 956–971 (2014).
15. **Navin, N., Kendall, J., Troge, J., Andrews, P., Rodgers, L., McIndoo, J., Cook, K., Stepansky, A., Levy, D., Esposito, D., and other 5 authors:** Tumour evolution inferred by single-cell sequencing, Nature, **472**, 90–94 (2011).
16. **Sun, Y., Haglund, T. A., Rogers, A. J., Ghanim, A. F., and Sethu, P.:** Review: microfluidics technologies for blood-based cancer liquid biopsies, Anal. Chim. Acta, **1012**, 10–29 (2018).
17. **Wang, Y. and Navin, N. E.:** Advances and applications of single-cell sequencing technologies, Mol. Cell, **58**, 598–609 (2015).
18. **Alberti, S., Stovel, R., and Herzenberg, L. A.:** Preservation of cells sorted individually onto microscope slides with a fluorescence-activated cell sorter, Cytometry, **5**, 644–647 (1984).
19. **Kunz, D. J., Gomes, T., and James, K. R.:** Immune cell dynamics unfolded by single-cell technologies, Front. Immunol., **9**, 1435 (2018).
20. **Proserpio, V. and Mahata, B.:** Single-cell technologies to study the immune system, Immunology, **147**, 133–140 (2016).
21. **Seah, Y. F. S., Hu, H., and Merten, C. A.:** Microfluidic single-cell technology in immunology and antibody screening, Mol. Aspect. Med., **59**, 47–61 (2018).
22. **Sinha, N., Subedi, N., and Tel, J.:** Integrating immunology and microfluidics for single immune cell analysis, Front. Immunol., **9**, 2373 (2018).
23. **Meyvantsson, I. and Beebe, D. J.:** Cell culture models in microfluidic systems, Annu. Rev. Anal. Chem., **1**, 423–449 (2008).
24. **Sackmann, E. K., Fulton, A. L., and Beebe, D. J.:** The present and future role of microfluidics in biomedical research, Nature, **507**, 181–189 (2014).
25. **Yi, C., Li, C.-W., Ji, S., and Yang, M.:** Microfluidics technology for manipulation and analysis of biological cells, Anal. Chim. Acta, **560**, 1–23 (2006).
26. **Aharoni, A., Amitai, G., Bernath, K., Magdassi, S., and Tawfik, D. S.:** High-throughput screening of enzyme libraries: thiolactonases evolved by fluorescence-activated sorting of single cells in emulsion compartments, Chem. Biol., **12**, 1281–1289 (2005).
27. **Aharoni, A., Griffiths, A. D., and Tawfik, D. S.:** High-throughput screens and selections of enzyme-encoding genes, Curr. Opin. Chem. Biol., **9**, 210–216 (2005).
28. **Griffiths, A. D. and Tawfik, D. S.:** Miniaturising the laboratory in emulsion droplets, Trends Biotechnol., **24**, 395–402 (2006).
29. **Cristini, V. and Renardy, Y.:** Scalings for droplet sizes in shear-driven breakup: non-microfluidic ways to monodisperse emulsions, Fluid Dyn. Mater. Process., **2**, 77–93 (2006).
30. **Xu, J. H., Luo, G. S., Li, S. W., and Chen, G. G.:** Shear force induced monodisperse droplet formation in a microfluidic device by controlling wetting properties, Lab Chip, **6**, 131–136 (2006).
31. **Varma, S. and Voldman, J.:** A cell-based sensor of fluid shear stress for microfluidics, Lab Chip, **15**, 1563–1573 (2015).
32. **Chattopadhyay, P. K., Gierahn, T. M., Roederer, M., and Love, J. C.:** Single-cell technologies for monitoring immune systems, Nat. Immunol., **15**, 128–135 (2014).
33. **DeKosky, B. J., Ippolito, G. C., Deschner, R. P., Lavinder, J. J., Wine, Y., Rawlings, B. M., Varadarajan, N., Giesecke, C., Dorner, T., Andrews, S. F., and other 5 authors:** High-throughput sequencing of the paired human immunoglobulin heavy and light chain repertoire, Nat. Biotechnol., **31**, 166–169 (2013).
34. **Furutani, S., Nagai, H., Takamura, Y., Aoyama, Y., and Kubo, I.:** Detection of expressed gene in isolated single cells in microchambers by a novel hot cell-direct RT-PCR method, Analyst, **137**, 2951–2957 (2012).
35. **Love, J. C., Ronan, J. L., Grotenbreg, G. M., van der Veen, A. G., and Ploegh, H. L.:** A microengraving method for rapid selection of single cells producing antigen-specific antibodies, Nat. Biotechnol., **24**, 703–707 (2006).
36. **Varadarajan, N., Kwon, D. S., Law, K. M., Ogunniyi, A. O., Anahtar, M. N., Richter, J. M., Walker, B. D., and Love, J. C.:** Rapid, efficient functional characterization and recovery of HIV-specific human $CD8^+$ T cells using microengraving, Proc. Natl. Acad. Sci. USA, **109**, 3885–3890 (2012).
37. **Chiu, D. T., deMello, A. J., Di Carlo, D., Doyle, P. S., Hansen, C., Maceiczyk, R. M., and Wootton, R. C. R.:** Small but perfectly formed? Successes, challenges, and opportunities for microfluidics in the chemical and biological sciences, Chem, **2**, 201–223 (2017).
38. **Du, G., Fang, Q., and den Toonder, J. M.:** Microfluidics for cell-based high throughput screening platforms - a review, Anal. Chim. Acta, **903**, 36–50 (2016).
39. **Haliburton, J. R., Shao, W., Deutschbauer, A., Arkin, A., and Abate, A. R.:** Genetic interaction mapping with microfluidic-based single cell sequencing, PLoS One, **12**, e0171302 (2017).
40. **Macosko, Evan Z., Basu, A., Satija, R., Nemesh, J., Shekhar, K., Goldman, M., Tirosh, I., Bialas, Allison R., Kamitaki, N., Martersteck, Emily M., and other 6 authors:** Highly parallel genome-wide expression profiling of individual cells using nanoliter droplets, Cell, **161**, 1202–1214 (2015).
41. **Prakadan, S. M., Shalek, A. K., and Weitz, D. A.:** Scaling by shrinking: empowering single-cell 'omics' with microfluidic devices, Nat. Rev. Genet., **18**, 345 (2017).
42. **Yao, X., Choudhury, A. D., Yamanaka, Y. J., Adalsteinsson, V. A., Gierahn, T. M., Williamson, C. A., Lamb, C. R., Taplin, M. E., Nakabayashi, M., Chabot, M. S., and other 7 authors:** Functional analysis of single cells identifies a rare subset of circulating tumor cells with malignant traits, Integr. Biol. (Camb), **6**, 388–398 (2014).
43. **Shalek, A. K., Satija, R., Shuga, J., Trombetta, J. J., Gennert, D., Lu, D., Chen, P., Gertner, R. S., Gaublomme, J. T., Yosef, N., and other 12 authors:** Single-cell RNA-seq reveals dynamic paracrine control of cellular variation, Nature, **510**, 363–369 (2014).
44. **Zeisel, A., Munoz-Manchado, A. B., Codeluppi, S., Lonnerberg, P., La Manno, G., Jureus, A., Marques, S., Munguba, H., He, L., Betsholtz, C., and other 4 authors:** Brain structure. Cell types in the mouse cortex and hippocampus revealed by single-cell RNA-seq, Science, **347**, 1138–1142 (2015).
45. **Treutlein, B., Brownfield, D. G., Wu, A. R., Neff, N. F., Mantalas, G. L., Espinoza, F. H., Desai, T. J., Krasnow, M. A., and Quake, S. R.:** Reconstructing lineage hierarchies of the distal lung epithelium using single-cell RNA-seq, Nature, **509**, 371–375 (2014).
46. **Patel, A. P., Tirosh, I., Trombetta, J. J., Shalek, A. K., Gillespie, S. M., Wakimoto, H., Cahill, D. P., Nahed, B. V., Curry, W. T., Martuza, R. L., and other 5 authors:** Single-cell RNA-seq highlights intratumoral heterogeneity in primary glioblastoma, Science, **344**, 1396–1401 (2014).
47. **Shalek, A. K., Satija, R., Adiconis, X., Gertner, R. S., Gaublomme, J. T., Raychowdhury, R., Schwartz, S., Yosef, N., Malboeuf, C., Lu, D., and other 8 authors:** Single-cell transcriptomics reveals bimodality in expression and splicing in immune cells, Nature, **498**, 236–240 (2013).
48. **Tirosh, I., Izar, B., Prakadan, S. M., Wadsworth, M. H., 2nd, Treacy, D., Trombetta, J. J., Rotem, A., Rodman, C., Lian, C., Murphy, G., and other 27 authors:** Dissecting the multicellular ecosystem of metastatic melanoma by single-cell RNA-seq, Science, **352**, 189–196 (2016).
49. **Shields, C. W. t., Reyes, C. D., and Lopez, G. P.:** Microfluidic cell sorting: a review of the advances in the separation of cells from debulking to rare cell isolation, Lab Chip, **15**, 1230–1249 (2015).
50. **Cao, R., Pankayatselvan, V., and Houston, J. P.:** Cytometric sorting based on the fluorescence lifetime of spectrally overlapping signals, Optic Express, **21**, 14816–14831 (2013).
51. **Picot, J., Guerin, C. L., Le Van Kim, C., and Boulanger, C. M.:** Flow cytometry: retrospective, fundamentals and recent instrumentation, Cytotechnology, **64**, 109–130 (2012).
52. **Bonner, W. A., Hulett, H. R., Sweet, R. G., and Herzenberg, L. A.:** Fluorescence activated cell sorting, Rev. Sci. Instrum., **43**, 404–409 (1972).
53. **DeKosky, B. J., Kojima, T., Rodin, A., Charab, W., Ippolito, G. C., Ellington, A. D., and Georgiou, G.:** In-depth determination and analysis of the human paired heavy- and light-chain antibody repertoire, Nat. Med., **21**, 86–91 (2015).
54. **McDaniel, J. R., DeKosky, B. J., Tanno, H., Ellington, A. D., and Georgiou, G.:** Ultra-high-throughput sequencing of the immune receptor repertoire from millions of lymphocytes, Nat. Protoc., **11**, 429–442 (2016).
55. **Wang, B., DeKosky, B. J., Timm, M. R., Lee, J., Normandin, E., Misasi, J., Kong, R., McDaniel, J. R., Delidakis, G., Leigh, K. E., and other 23 authors:** Functional interrogation and mining of natively paired human VH:VL antibody repertoires, Nat. Biotechnol., **36**, 152–155 (2018).
56. **McDaniel, J. R., Pero, S. C., Voss, W. N., Shukla, G. S., Sun, Y., Schaetzle, S., Lee, C. H., Horton, A. P., Harlow, S., Gollihar, J., and other 7 authors:** Identification of tumor-reactive B cells and systemic IgG in breast cancer based on clonal frequency in the sentinel lymph node, Cancer Immunol. Immunother., **67**, 729–738 (2018).
57. **Ye, J., Ma, N., Madden, T. L., and Ostell, J. M.:** IgBLAST: an immunoglobulin variable domain sequence analysis tool, Nucleic Acids Res., **41**, W34–W40 (2013).
58. **Rognes, T., Flouri, T., Nichols, B., Quince, C., and Mahe, F.:** VSEARCH: a versatile open source tool for metagenomics, PeerJ, **4**, e2584 (2016).
59. **Rayleigh, L.:** On the instability of jets, Proc. Lond. Math. Soc., **s1–10**, 4–13 (1878).
60. **Rayleigh, L.:** XX. On the equilibrium of liquid conducting masses charged with electricity, Lond. Edinb. Dublin Phil. Mag. J. Sci., **14**, 184–186 (1882).
61. **Georgiou, G., Ippolito, G. C., Beausang, J., Busse, C. E., Wardemann, H., and Quake, S. R.:** The promise and challenge of high-throughput sequencing of the antibody repertoire, Nat. Biotechnol., **32**, 158–168 (2014).
62. **Wilson, P. C. and Andrews, S. F.:** Tools to therapeutically harness the human antibody response, Nat. Rev. Immunol., **12**, 709–719 (2012).

63. **Turchaninova, M. A., Britanova, O. V., Bolotin, D. A., Shugay, M., Putintseva, E. V., Staroverov, D. B., Sharonov, G., Shcherbo, D., Zvyagin, I. V., Mamedov, I. Z., and other 3 authors:** Pairing of T-cell receptor chains via emulsion PCR, Eur. J. Immunol., **43**, 2507–2515 (2013).
64. **Headen, D. M., García, J. R., and García, A. J.:** Parallel droplet microfluidics for high throughput cell encapsulation and synthetic microgel generation, Microsyst. Nanoeng., **4**, 17076 (2018).
65. **Li, W., Young, E. W. K., Seo, M., Nie, Z., Garstecki, P., Simmons, C. A., and Kumacheva, E.:** Simultaneous generation of droplets with different dimensions in parallel integrated microfluidic droplet generators, Soft Matter, **4**, 258–262 (2008).
66. **Sidore, A. M., Lan, F., Lim, S. W., and Abate, A. R.:** Enhanced sequencing coverage with digital droplet multiple displacement amplification, Nucleic Acids Res., **44**, e66 (2016).
67. **Byrnes, S. A., Chang, T. C., Huynh, T., Astashkina, A., Weigl, B. H., and Nichols, K. P.:** Simple polydisperse droplet emulsion polymerase chain reaction with statistical volumetric correction compared with microfluidic droplet digital polymerase chain reaction, Anal. Chem., **90**, 9374–9380 (2018).